

# Electrically controlled waveguide polariton laser

D. G. Suárez-Forero,<sup>1</sup> F. Riminucci,<sup>2,3</sup> V. Ardizzone,<sup>1,\*</sup> M. de Giorgi,<sup>1</sup> L. Dominici,<sup>1</sup>  
F. Todisco,<sup>1</sup> G. Lerario,<sup>1</sup> L. N. Pfeiffer,<sup>4</sup> G. Gigli,<sup>2</sup> D. Ballarini,<sup>1</sup> and D. Sanvitto<sup>1,†</sup>

<sup>1</sup>*CNR NANOTEC, Institute of Nanotechnology, Via Monteroni, 73100 Lecce, Italy*

<sup>2</sup>*Dipartimento di Fisica, Università del Salento, Strada Provinciale Lecce-Monteroni, Campus Ecotekne, Lecce 73100, Italy*

<sup>3</sup>*Molecular Foundry, Lawrence Berkeley National Laboratory,  
One Cyclotron Road, Berkeley, California, 94720, USA*

<sup>4</sup>*PRISM, Princeton Institute for the Science and Technology of Materials, Princeton University, Princeton, NJ 08540*

Semiconductor polariton systems offer a versatile solid state platform to study many-body physical effects such as lasing or superfluidity in out-of-equilibrium systems. They are also anticipated as a new platform for integrated optics: behaving as interacting photons, these mixed light-matter quasi-particles could be the cornerstone of a new technology for optoelectronic devices, implementing logic gates, switches and other functionalities. In this work we demonstrate an electrically controlled polariton laser, in a compact, easy-to-fabricate and integrable configuration, based on a semiconductor waveguide. Interestingly, we show that polariton lasing can be achieved in a system without a local minimum in the polariton energy-momentum dispersion. The surface cavity modes for the laser emission are obtained by adding couples of specifically designed diffraction gratings on top of the planar waveguide, forming an in-plane Fabry-Perot cavity. It is thanks to the waveguide geometry, that we can apply a transverse electric field in order to finely tune the laser energy and quality factor of the cavity modes. Remarkably, we exploit the system sensitivity to the applied electric field to achieve an electrically switched source of coherent polaritons. The precise control that can be reached with the manipulation of the grating properties and of the electric field, provide strong advantages to this device in terms of miniaturization and integrability, two main features for the future development of coherent sources from polaritonic technologies.

## INTRODUCTION

A semiconductor system in which a photon emitted from an active medium has a larger probability of being reabsorbed than that of escaping out of the optical resonator, is called to be in strong coupling. This condition translates for the formation of the so called exciton polariton: a light-matter quasi-particle resulting from the hybridization between an electromagnetic cavity mode and an exciton dipole in a semiconductor [1]. Since the first observation [2], polaritonic systems have become a suitable platform to study fundamental physical phenomena; effects such as optical parametric oscillations [3], bistability [4], Bose-Einstein condensation [5, 6], superfluidity [7, 8] and quantum vorticity [9] are some of the most intriguing phenomena that have been demonstrated. Peculiar features of polaritons such as long coherence time and high nonlinearities are chased for the realization of integrated optical elements [10]. Experimental devices such as polariton transistors [11] and routers [12] have indeed shown their viability for all-optical logic systems. More recently, the generation and manipulation of polaritons at the single or few particles level, have been reported [13–15], in an effort to assess the potential of these systems as a platform for quantum information processing.

The so called “polariton laser” [16] is one of the most paradigmatic effects observed in strongly coupled systems. This phenomenon is observed when a phase transition to a coherent state of polaritons takes place above a critical density. It has been demonstrated in systems such as semiconductor, organic or hybrid microcavities [17–24] and photonic crystal cavities [25–27]. From this point of view, optical waveguides (WG) represent a very attractive platform for the exploitation of this effect in actual devices, due to an easy technological fabrication, the high quality factors achievable and the particular geometry, suitable for the integration of polaritonic optical circuits and coherent optical sources. A guided electromagnetic mode, localized in the two dimensional plane of the WG by total internal reflection, couples to an exciton which is confined to the quantum well (QW), giving rise to WG polariton modes [28, 29], in counterposition to the more reknown microcavity polariton modes [1]. Recently, new WG designs have enabled the application of a transverse electric field, while keeping the system in the strong coupling regime [28, 30]. We indeed show that, despite the lack of an energy minimum in the WG polariton dispersion, an electrically controlled polariton lasing effect can be achieved even with guided polaritons propagating at high speed.

We use two metal gratings placed on top of the GaAs/AlGaAs slab, that behave like a couple of semi-reflective mirrors, confining the WG polariton mode, and furthermore to outcouple the laser emission vertically throughout one of their diffraction orders. Their design favors the formation of an energy gap in the energy momentum dispersion of the planar WG mode. Inside this energy interval, a manifold of Fabry-Perot (FP) modes is formed by the cavity

effect between the gratings, funneling the light absorbed and reemitted by carrier recombinations under the pump spot. The lasing effect is then enabled on a specific polariton mode, i.e., the first mode for which gain equals losses upon increasing pump power. Parameters such as grating periodicity and filling factor as well as the cavity length (i.e. distance between gratings) provide a fine control of the laser properties, without the need for complex postprocessing of the WG. Most importantly, using an electric field applied in the direction perpendicular to the WG plane, we demonstrate real-time tunability of the emission wavelength. We stress that this electrical control is possible only because of the WG geometry, that allows to place the electrodes in close vicinity to the quantum wells, as it has been previously reported on the same structure [28, 30, 31]. The strong coupling regime and the sensitivity of the exciton to the externally applied electric field allow us to obtain an electrically controlled source of coherent polaritons, realizing electro-switching with ultra-high figures of merit. Based on these findings, the coherent, electrically controlled polaritons source demonstrated here could be an important tool for future polariton circuits, enabling functionalities such as electrical injection, Q-switch lasers, electro-optic modulators and configurable logic gates.

## RESULTS

The WG structure is grown on an  $n^+$ -doped GaAs substrate, on top of which a 500 nm cladding of  $Al_{0.8}Ga_{0.2}As$  was previously deposited [28, 30, 31]. The structure consists of 12 pairs of 20 nm thick GaAs quantum wells (QW) separated by 20 nm of  $Al_{0.4}Ga_{0.6}As$  barriers. Light is extracted through gold gratings spaced by a distance ranging from 50  $\mu m$  to 150  $\mu m$ . To realize FP resonators inside the WG, two identical gratings are fabricated facing each other on top of the slab at a given distance along their line of sight (a sketch of the full system is shown in Fig. 1a and the calculated spatial distribution of the electric field in-plane component is depicted in Fig. 1b). We use gratings with pitch  $\sim 240$  nm and filling factor comprised between  $\sim 0.72$  and  $\sim 0.85$ . Finally, a 50 nm layer of ITO is sputtered on top of the sample. This layer, together with the doped substrate in the opposite side, allows for the application of an electric field in a direction perpendicular to the slab plane. The purpose of the electric field is to tune the exciton energy, exploiting the Stark effect, and hence its influence on the polaritonic guided modes [28, 30, 31]. A more detailed description of the structure is given in the Materials and Methods section.

To firstly verify the presence and features of the WG modes inside the slab, we use a nonresonant pump laser which excites the sample outside of the gratings region, while the photoluminescence (PL) spectrum of the system is collected through an individual grating (so no cavity is formed) placed 100  $\mu m$  away from the off-resonant excitation spot. Figures 1c-d show the PL emission coming from the hybridized zero-th order Transverse Magnetic (TM) and Transverse Electric (TE) modes of the structure, respectively. The dispersions are plotted as a function of the wavevector  $\beta$  of the propagating mode inside the slab. The uncoupled bare exciton line (heavy hole exciton) and guided optical modes are indicated by horizontal and oblique red dashed lines, respectively. The experimental polariton dispersion can be fitted by means of a theoretical model of coupled oscillators, as shown by the solid lines in Fig. 1c-d. The results show an asymmetry in the Rabi splitting ( $\Omega$ ) between the TE and TM modes. We obtain values of 13.4 meV and 5.2 meV, respectively. As a matter of fact this is predicted by the selection rules for the coupling of the confined modes with the exciton dipole, which imply an  $\Omega$  value around three times higher for the TE mode than for the TM mode, as it has already been observed in similar samples [28, 32]. The figure also evidences an important difference in the wavevector  $\beta$  spreading between the TM and the TE modes. This linewidth effect is originated by the different grating efficiency with respect to each polarization and it is correlated with the formation of the FP cavity inside the structure, as will be described in detail in the Discussion Section.

After the WG modes, we also characterize the features of the top gratings and their role in forming the the FP cavity. Figure 2a shows the angle-integrated PL emission intensity from the terminal end of a single and very extended, 400  $\mu m$ -long grating as a function of the emission energy. Both the TE and TM polarization possess a local minimum in the emitted intensities, highlighted by vertical arrows in the figure. These minima represent energy gaps corresponding to wavevectors of the guided modes that are back-reflected by the grating. In other words, each grating acts as a mirror in the energy interval corresponding to the gaps of Fig. 2a and, when two gratings face each other, a planar FP cavity is formed, with a cavity length which depends on the distance  $L$  between gratings. The cavity modes are characterized now thanks to the PL emission outcoupled from one of the gratings when a nonresonant pumping spot is placed in the middle between the two (as illustrated in Fig. 1a). Figure 2b shows the PL emission of the cavity modes formed along the  $TM_0$  mode by placing the gratings at distances of  $L = 50$   $\mu m$  (black upper line),  $L = 100$   $\mu m$  (middle blue line) and  $L = 150$   $\mu m$  (lower red line). As expected, the closer the gratings to each other, the larger the free spectral range. In the case of the gratings separated by 50  $\mu m$  the modes spacing is  $\sim 2.3$  meV that corresponds to the FP mode of manifold 17. For the case of a pair of gratings separated 100  $\mu m$ , the spacing is  $\sim 1.4$

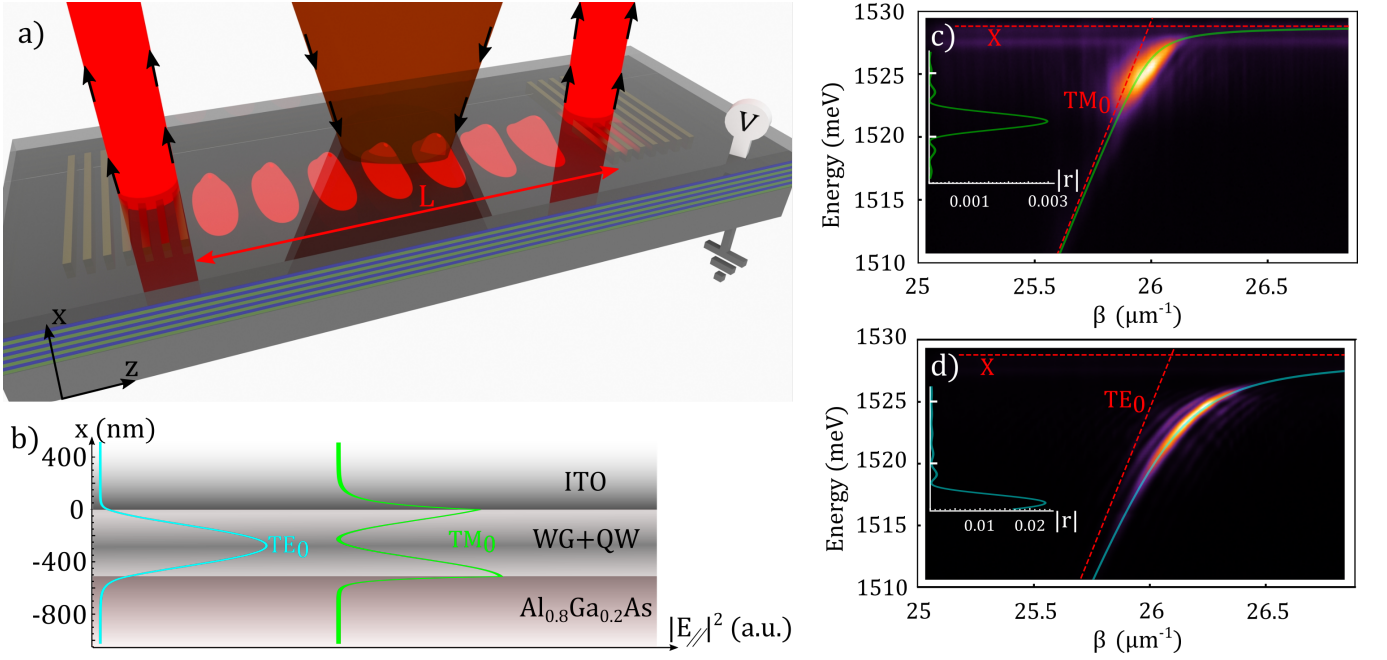


FIG. 1. **a** Schematic representation of the system. Two gold gratings, placed on top of the WG, couple to the vanishing tail of the guided modes. As a result, a FP cavity is formed inside the slab for the TM mode, opening the possibility to observe a lasing effect in the system.  $L$  is the cavity length given by the distance between the gratings. The doped substrate, together with a top layer of ITO, enables the application of an electric field in the direction perpendicular to the cavity plane. **b** Calculated intensity profile of the in-plane electric field for each guided mode. The  $x$  component of the electric field for the  $TM_0$  mode is not included in the scheme because it does not contribute to the light-matter coupling. **c-d** Polarization resolved PL dispersion of the system extracted through a single gold grating placed on top of the slab WG. Each dispersion is plotted as a function of the wavevector of the guided modes  $\beta$ . Panel c corresponds to TM polarization, while panel d shows the dispersion for the TE mode. Continuous lines correspond to a fitting of each mode by using a theoretical model of coupled oscillators. The obtained Rabi splitting ( $\Omega$ ) values are 5.2 meV for the TM mode and 13.4 meV for the TE. The bare exciton and photonic modes are indicated by red dashed lines. The calculated reflectivity of the mode in presence of the grating is displayed as an inset for each polarization. The creation of reflectivity maxima indicates the opening of energy gaps.

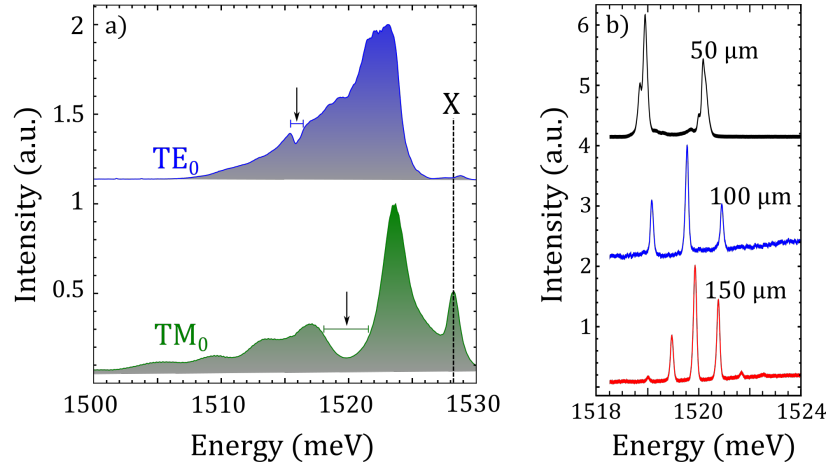


FIG. 2. **a** Experimental measurement of the gratings gap in TE and TM polarization. The spectra are obtained by integrating the PL emission from the terminal end of a  $400\text{ }\mu\text{m}$ -long gold grating over the emission angle. The vertical dashed line indicates the exciton energy. The opening of two bandgaps is highlighted by the vertical arrows. **b** Fabry-Pérot modes formed along the  $TM_0$  dispersion. The constructed FP cavities have different lengths, determined by the distance between the gratings. As expected for an optical cavity, the smaller the cavity, the greater the free spectral range at a given energy. The spectral distances of 2.3 meV for the cavity of length  $50\text{ }\mu\text{m}$ , 1.4 meV for the cavity of  $100\text{ }\mu\text{m}$  and 0.9 meV for the cavity of  $150\text{ }\mu\text{m}$ , are associated to FP modes of manifold 17, 30 and 45, respectively.

meV (manifold 30) and for the gratings separated  $150\text{ }\mu\text{m}$  the spacing is  $\sim 0.9\text{ meV}$  (manifold 45). The observed FP modes are then an effect of the confinement of the  $\text{TM}_0$  mode due to the presence of two identical gratings. A comparative analysis of the extracted PL is performed with respect to the fabrication and materials features of the grating(s) (Fig. S4) and shows that when the metallic grating is in direct contact with the dielectric guide it carries a considerable spectral broadening of the measured TM mode (and not of TE one). We assign this broadening to an additional residual absorption from plasmonic modes in the gold grating, a widely studied effect [33–36]. It is important to note that this possible plasmon induced absorption takes place only in the grating region and does not modify the truly waveguide polariton character of the propagating modes outside the gratings, as demonstrated in Fig. S4c, where the PL emission collected through a fully dielectric grating confirms the expected behavior for a system operating in the strong coupling regime. For an extended discussion with respect to the grating features, we refer the reader to the SM.

We have characterized all the three building blocks (namely the WG modes, the gratings and the planar FP cavity), which are mandatory for the observation of the waveguiding lasing effect. We can hence shine a high peak-power nonresonant laser in a region between the two gratings, in the specific we use a 100 fs pulsed laser tuned at 1.59 eV ( $\approx 780\text{ nm}$ ) and 80 Mhz repetition rate, with a spot size of  $40\text{ }\mu\text{m}$ . Figure 3a shows the P-L emission in real space at threshold excitation power. The big spot between the gratings corresponds to the exciton emission under the pump spot which is not coupled to the guided modes. The excited guided polariton modes propagate along the slab with in-plane vector  $\beta$  and are partly extracted and partly reflected back in the plane when they hit the gratings, highlighted by white rectangles. The PL emission extracted from grating 1 can be resolved in both energy and momentum (Fig. 3b). Remarkably, such emission shows a series of discrete peaks along the TM polariton dispersion corresponding to the FP modes of Fig. 2b. In other words, in the region of space comprised between the two identical gratings, a FP cavity is formed, sustaining the discrete modes observed in Fig. 3b. With increasing pump power, as shown in Fig. 3c-d, the system shows a clear threshold behaviour (see inset of panel d) with prominent coherent emission from only one of the FP modes at an energy of  $\sim 1520.5\text{ meV}$ , that in the dispersion relation corresponds to a wavevector  $\beta = 25.96\text{ }\mu\text{m}^{-1}$ . This is the precise in-plane wavelength corresponding to the grating pitch  $\Lambda$ , where it is hence maximally reflective. When the emitted light from the two gratings is overlapped in  $k$  space, an interference pattern is generated (Fig. S5b). Moreover, a strong reduction of the linewidth of the FP mode is observed across the lasing threshold (Fig. S5a). The threshold and linewidth effects are clear signatures which mark the onset of the lasing regime in the system. We gain an even better insight into the laser emission build-up, upon accessing the temporal dynamics of the process by means of a streak camera coupled to a monochromator and a scan in the reciprocal space. The energy momentum dispersion resolved at different time frames of the dynamics is shown in the Supplementary Video 1 and discussed in the Supplementary Material (SM), along with a detailed screenshot in Fig. S6. In this case the pump spot is placed between the two gratings and the emission from one of the gratings is recorded. The temporal reconstruction reveals that the build-up necessary to reach the inversion of population (i.e., the start of the lasing emission) occurs 200 ps after the pulse arrival (see Discussion section). In the Supplementary Video 2 we show the dynamics of the system measured under the pumping laser, by placing its spot on one of the two gratings and imaging the emission from both (see Figs. S1 and S7 for experimental details). The video shows that under the pumping spot the strong exciton-photon coupling is lost when the excitation pulse arrives, essentially due to the high density of photo-generated carriers, and then is slowly recovered after the lasing action is over. The system is excited at threshold, which explains why several FP modes are still visible. On the lower part of the image, the TE polariton mode is also visible; however, this mode comes from the grating at the opposite side of the excitation spot, thus always in the strong coupling regime. A screenshot taken from each video is reproduced and detailed in the SM, Figs. S6 and S7.

Finally, we can now apply an external electric field perpendicular to the plane of the slab, demonstrating an extra degree of freedom acting as an additional control parameter on the WG polariton lasing. Figure 4a shows the spectra obtained from the TM polariton dispersion at  $\beta \approx 26\text{ }\mu\text{m}^{-1}$  and for different applied voltages. The TM dispersion is modified due to the Stark effect that red-shifts the exciton energy, providing a tool for a fine tuning of the laser energy in real time. In Fig. 4b-c we measure the central emission energy and the linewidth of the lasing mode for three different applied voltages and as a function of the pump power. For small applied fields ( $\leq 0.9\text{ V}$ ), a red-shift of the lasing mode is observed. When the applied electric field is further increased ( $> 0.9\text{ V}$ ), the exciton energy approaches the cavity modes, more largely altering their absorption properties, and hence, their relative losses. As a matter of fact, Fig. 4d shows that for an applied voltage of 1.5 V, the mode in which the stimulated emission takes place jumps to the next manifold (both spectra are taken at threshold power). The electric field acts in this case as a neat switch that allows to select the mode in which the lasing takes place by modifying the FP modes relative losses. The inset of Fig. 4d shows the evolution of the linewidths of the two lasing peaks upon application of the electric field. Indeed the switch between the lasing modes also coincides with the crossing of their linewidths.

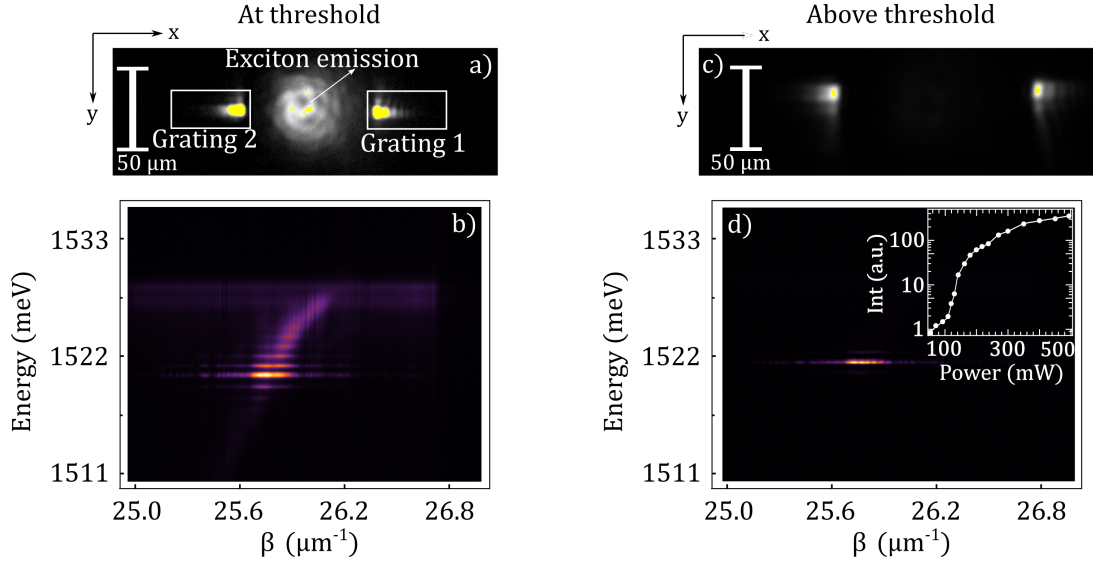


FIG. 3. **a** Real space image of the system when excited out of resonance at the threshold power. The laser spot is placed in the middle of the FP cavity, exciting both, the QW exciton with low in-plane momentum (central spot) and the polaritonic guided modes, extracted from the gratings (indicated with white rectangles). The residual pump laser signal is suppressed with a long-pass spectral filter. **b** The TM mode is reconstructed in the Fourier space by spatially isolating the PL from grating 1. The insertion of the gratings entails an additional confinement, and hence, the formation of discrete modes along the TM dispersion, as it can be observed in the image. **c** When the pump power overcomes the threshold, one mode of the cavity gets massively populated, reaching an emission intensity much higher than any other emission in the system. **d** the PL dispersion measurement (measured as in **b**) confirms which state of the FP cavity gets populated. The inset in **d** shows the intensity of the lasing mode as a function of the pumping power; a clear threshold behaviour is visible.

## DISCUSSION

We demonstrated the design and realisation of a micrometer size laser in a GaAs/AlGaAs polariton-WG by using two metallic gratings at controlled distance on top of the slab WG, in order to form a FP cavity that confines the photonic field in one dimension. To better understand this effect, we calculate the influence of the grating on the guided modes by using a perturbation formalism to study the coupling between counter-propagating modes [37, 38]. For a WG grown in the  $x$  direction, and with modes propagating in the  $z$  direction, the magnetic field  $H(x, z, t)$  of the  $m^{th}$  TM mode, can be expressed in case of an infinite slab in the  $y$  direction (i. e.  $d/dy = 0$ ) as:

$$H_m(x, z, t) = \mathcal{H}_y^m(x) e^{i(\omega t - \beta_m z)} \quad (1)$$

Where  $\mathcal{H}(x)$  is derived from the corresponding wave equation and boundary conditions under the “long wavelength” approximation, that takes into account the internal WG periodicity (12 pairs of QW+barrier) by considering an effective refractive index. A numerical verification of the validity of this approach, upon comparison with a full transfer matrix method, is presented and discussed in Fig. S2 of the SM, together with its detailed explanation, based on ref. [39]. The fabrication of a grating with periodicity  $\Lambda$  on top of the WG acts as a perturbation that changes the effective in-plane momentum of the  $m^{th}$  mode as:

$$\beta'_m = \frac{l\pi}{\Lambda} - \sqrt{\left(\beta_m - \frac{l\pi}{\Lambda}\right)^2 - |\kappa|^2} \quad (2)$$

With  $\beta_m$  the in-plane momentum of the unperturbed  $m^{th}$  mode,  $l$  an integer number such as  $|\beta_m - \frac{l\pi}{\Lambda}| \sim 0$  and  $\kappa$  a constant that depends on the grating periodicity and material, and the spatial profile of the transverse field. In the case of a square grating fabricated on top of the slab, with filling factor  $a$ , height  $h$  and refractive index  $n_g$ , the constant  $\kappa$  takes the form

$$\kappa = \frac{i\omega\mu_o}{4\pi l} \text{Sin}(\pi l a) \int_0^h \left( (n_g/n_{ITO})^2 - 1 \right) [\mathcal{H}_y^m(x)]^2 dx \quad (3)$$

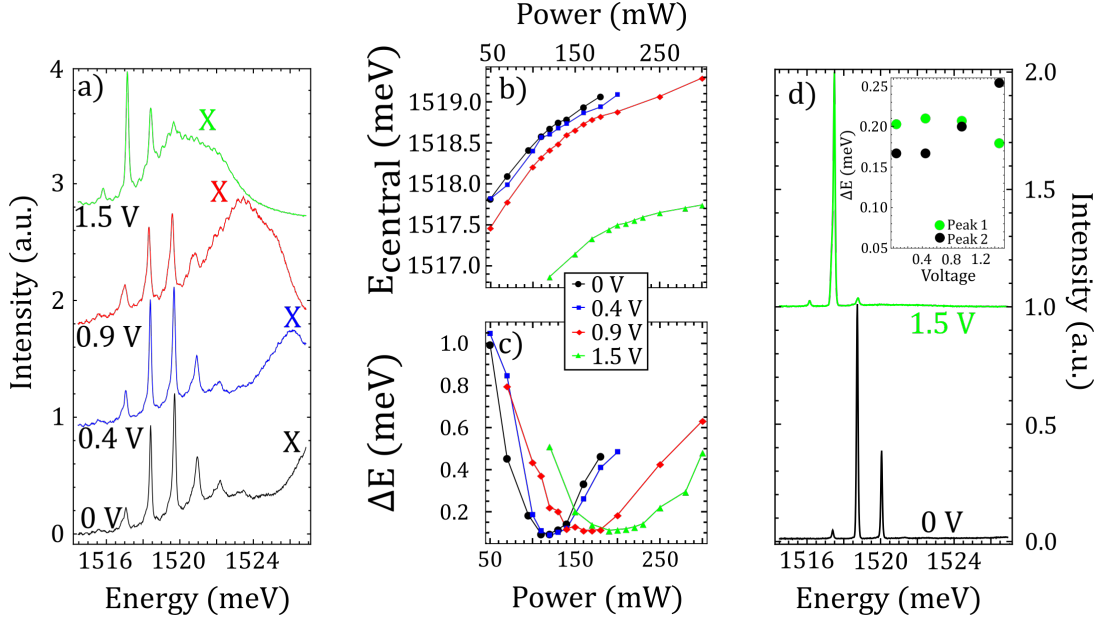


FIG. 4. **a** Spectra obtained by cutting the TM polariton dispersion at  $\beta \approx 26\mu\text{m}^{-1}$  and for different applied voltages. The letter X indicates the peak corresponding to the PL emission of the uncoupled exciton that redshifts due to the Stark effect. **b-c** To verify that the presence of a transverse electric field does not affect the properties of the lasing effect, we verify the central energy shift (b) and spectral narrowing (c) for three applied voltages. The results not only confirm the lasing effect in every case, but show that the electric field acts as a fine tuning of the laser energy for small voltages through the Stark shift of the exciton, and as a switch that allows to select the cavity mode in which the lasing takes place. The latter effect is achieved as a consequence of a modification of the relative Q factor of the cavity modes, since the exciton resonance affects the absorption at the energy of each FP mode. **d** Spectra of the cavity taken at threshold power without any transverse electric field (black) and with an applied voltage of 1.5 V (blue). The modes energy is almost unaltered, but the change of their absorption properties switches the mode in which the stimulated emission takes place. The inset shows the FWHM of each peak as the applied electric field increases. When the quality factor of peak 1 decreases below the one of peak 2, the lasing mode switches.

This expression indicates the existence of an energy gap in the guided mode dispersion in the region covered by the grating when  $|\kappa|^2 > (\beta_m - \frac{l\pi}{\Lambda})^2$ . At the energy interval around the exciton ( $\sim 1.529$  meV), where the electromagnetic field hybridizes, the in-plane linear momentum of the TM guided mode lies in the range ( $25.6 \mu\text{m}^{-1} < \beta_m < 26.3 \mu\text{m}^{-1}$ ), as observed in Fig. 1c. For a grating with a period of  $\Lambda = 243$  nm, the condition  $\beta_m - \frac{l\pi}{\Lambda} \sim 0$  is satisfied for  $l = 2$ . The expressions 3 show that, for  $l$  even,  $\kappa$  differs from zero only for filling factors different than 0.5. Moreover it is also evident from the expressions that for  $l = 2$  the maximum gap's amplitude is obtained for a filling factor either 0.25 or 0.75. In our case, we fabricated gold gratings with filling factor close to 0.75 to maximize the coupling between propagating and counter-propagating modes and hence their reflectivity, whose calculation is shown on the left side of Figs. 1c-d. The Purcell enhancement effect induced by the semi-reflective gratings provides the conditions for the lasing from the FP mode with energy  $E \sim 1520.5$  meV and in-plane wavevector  $\beta \sim 25.96 \mu\text{m}^{-1}$  (Fig. 3d). The theoretical dispersion fitting reveals that the excitonic fraction of the coherent polariton population is  $|C_x|^2 = 0.1$ . An attractive feature of this system is that the excitonic component of the generated coherent population can be tailored by engineering the parameters of the FP cavity; in particular its length (distance between gratings) and the grating period. Hence, no modification of the slab WG is required.

It is worth noting that the blueshift of Fig. 4b cannot be simply associated to polariton-polariton interactions, since the exciton energy remains almost unaltered when the pump power is increased. It rather might depend on a local carrier-induced reduction of the WG refractive index [40], due, for example, to the plasma generated by the optical pump pulse, i. e., a plasma induced transparency [41, 42] or to the band filling effect. Such effects can be especially relevant in the spatial region below the pump spot. An estimation of the minimum index change necessary to account for the observed blueshift with increasing pump power can be done by considering that the  $i^{\text{th}}$  mode of the resonator has energy  $E_i = i \frac{h \cdot c}{2Ln}$ , where  $L$  is the cavity length, given by the distance between the gratings,  $n$  its effective refractive index,  $h$  the Planck's constant and  $c$  the vacuum light speed. The data shows a saturation behavior compatible with such explanation, with a reduction of only  $10^{-4}$  in the refractive index. Figure 4c shows the linewidth for different pump powers and voltages. The observed spectral narrowing at threshold is expected and

it is associated to the fact that the coherence time of the system exceeds the radiative lifetime of the confined mode under these excitation conditions [17]. Based on the optical characterization of the system and the complex temporal dynamics that we observe in the Supplementary Videos 1 and 2, we can explain the laser build-up in the following way: the gain media (QWs) are populated through the non-resonant pump in the middle of the FP cavity, as shown in Fig. 3a, forming an electronic plasma localized under the pumping spot. After the recombination of photo-created carriers, the photons can be emitted in any of these FP modes (as the Purcell factor enhances the emission in them). By following the standard laser theory [43] the first mode to start to lase is the one for which a threshold condition is met. This condition is written in terms of the critical population inversion:  $N_C = \gamma/\sigma L$ ; where  $N_C$  is the population at which the lasing starts and  $\sigma$  is the spontaneous emission coefficient. Here  $\gamma$  represents the overall losses of a given mode as  $\gamma = -\ln(R_1) - \ln(R_2) - \ln(1 - L)$  in which  $R_1$  and  $R_2$  are the mirror reflectivity and  $L$  represents the losses for a roundtrip in the cavity. The first mode to start to lase is then the mode with the smaller  $N_C$ , i.e., the mode with the smaller linewidth in the set of the FP modes created by the two gratings. By modifying the linewidth of the modes, as it is shown in Fig. 4d, it is possible to change the mode which starts to lase. It is important to remark that while the mechanism of the laser can be simply explained, the coherent population generated has an interactive nature, which could carry some complex effects of competition between modes, perhaps involving polariton nonlinearities. While these effect could be interesting they are beyond the scope of the present work. An additional feature revealed by the Supplementary Video 2 and Fig. S7 is the particular coexistence between populations in strong and weak coupling inside the FP cavity. While we detect complex emission patterns under the laser spot, that can be identified as carrier recombination in weak coupling regime, the emission from the grating corresponds to a WG polaritonic dispersion in strong coupling. This evidence goes in the direction of the creation of an electronic plasma under the pump spot, corresponding to an inversion of population. However, this plasma is restricted exclusively to the illuminated region (since the excitonic group velocity is too low to provide significant propagation). The radiative decay of this population into the polaritonic guided mode of the FP cavity with the lowest losses enables the massive population of such state, creating the coherent state of guided polaritons. The full process can then be interpreted as the coexistence of an electronic gas (in weak coupling) that preferably decays into a polaritonic guided mode, generating a coherent population of propagating hybrid light-matter particles (in strong coupling). We note also that recently a polariton laser effect has been claimed at both cryogenic and room temperature in ZnO based WGs [44]. In that case, the polariton emission has been interpreted as a standard polariton laser without need for a population inversion. While this interpretation can be supported by the large Rabi splitting observed in ZnO systems, our present work shows that in guided polariton systems an alternative interpretation can explain the same features. Moreover the absence of a blueshift in case of Ref. [44] could be also compatible with a refractive index change in the region between the two cracks. A careful check of the dynamics both below and outside the pumping region is essential in this kind of systems to better clarify the lasing mechanism involved.

In summary, we report a lasing effect providing a coherent source of high-speed, guided polaritons. The additional optical confinement necessary to achieve the laser emission is provided by placing two specifically designed gold gratings on top of the WG. It is worth to note that this design is versatile, easy-to-fabricate and does not require complex post-processing of the WG, such as vertical selective etching. Most important, thanks to the WG geometry, we demonstrate an effective electrical control of the vertical laser emission. Remarkably, by electrically tuning the quality factor of the modes, we obtain an electrically switched polariton laser. This effect could be exploited for the realization of electrically Q-switched sources of polaritons. More generally, the lasing effect we report in this work would allow the construction of tunable, micrometer-size coherent sources of polaritons with different properties in a single wafer of slab WG. These kind of optical sources could be valuable in polaritonics especially in the development of polaritonic circuits and integrated polaritonic logic elements.

## MATERIALS AND METHODS

**Waveguide sample** The full structure is grown on top of an  $n^+$ -doped GaAs substrate 500  $\mu\text{m}$  thick. The cladding layer is made of 500 nm of  $\text{Al}_{0.8}\text{Ga}_{0.2}\text{As}$ , while the WG is composed by 12 bilayers of  $\text{Al}_{0.4}\text{Ga}_{0.2}\text{As}$  barrier (20 nm thick) and GaAs QW (20 nm thick), and a final bilayer made of 20 nm of  $\text{Al}_{0.4}\text{Ga}_{0.2}\text{As}$  and 10 nm of GaAs.

**Fabrication of gold gratings and deposition of ITO** In order to fabricate gold gratings onto the sample we relied on a lift-off process. By design, they are 100  $\mu\text{m}$  long, 50  $\mu\text{m}$  wide and have a pitch of 243 nm. Their production requires a positive e-beam resist PMMA A4 to be spun at 4000 rpm onto the sample and baked for three minutes at 180  $^\circ\text{C}$ . The latter is then exposed using Raith150 and developed in MIBK:IPA 1:3. Subsequently, 3 nm



of chromium and 30 nm of gold are thermally evaporated. The sample is placed in Remover PG at approximately 80 °C to remove the resist. A SEM characterization of the obtained gratings is displayed and discussed in the SM (Fig. S3). The dense pattern carries irregularities in the first few grating wires related to the “proximity effect” [45], very common in electron beam lithography. As shown and discussed in Fig. S3, the affected area is negligible with respect to the full grating sizes. In closing, the electric contact is obtained by uniformly sputtering 50 nm of Indium Tin Oxide (ITO) on top of the sample; the gold grating results completely covered in the end.

**Optical measurements** For all the optical characterization the sample is kept at cryogenic temperature of 4 K. All the PL measurements are realized in a confocal configuration, using a 100 fs pulsed laser with a repetition rate of 80 MHz, tuned at 1.59 eV ( $\approx 780$  nm) to excite the sample out of resonance. The detection system allows to reconstruct either real or Fourier spaces in a Charge Coupled Device (CCD) coupled to a monochromator 70 cm long with a diffractive grating with either 600 or 1800 lines per mm. This way it is possible to perform measurements resolved in space, angle and energy. An image of the real space is reconstructed before the CCD in order to apply a spatial filter by using a slit, enabling the selection of one or both gratings. The residual laser signal is suppressed with a long-pass spectral filter at 1.55 eV ( $\approx 800$  nm). The time resolved images are performed in the same configuration, but directing the signal into a streak camera after passing the monochromator. The temporal reconstruction of the far field resolved in energy is made by moving vertically the focusing lens with a motorized station before it reaches the streak camera. Further details on the experimental setup and its schematic representation are presented in the SM.

### Acknowledgments

We thank Paolo Cazzato for the technical support.

We are grateful to R. Rapaport for inspiring discussions and for sharing information about the sample design.

Work at the Molecular Foundry was supported by the Office of Science, Office of Basic Energy Sciences, of the U.S. Department of Energy under Contract No. DE-AC02-05CH11231.

We acknowledge the project FISIR - C.N.R. Tecnopolo di nanotecnologia e fotonica per la medicina di precisione - CUP B83B17000010001 and ”Progetto Tecnopolo per la Medicina di precisione, Deliberazione della Giunta Regionale n. 2117 del 21/11/2018.

---

\* v.ardizzone85@gmail.com

† daniele.sanvitto@nanotec.cnr.it

- [1] Alexey Kavokin, Jeremy J. Baumberg, Guillaume Malpuech, and Fabrice P. Laussy. *Microcavities*. Oxford Science, second edition, 2008.
- [2] C. Weisbuch, M. Nishioka, A. Ishikawa, and Y. Arakawa. Observation of the coupled exciton-photon mode splitting in a semiconductor quantum microcavity. *Phys. Rev. Lett.*, 69:3314–3317, Dec 1992.
- [3] J. J. Baumberg, P. G. Savvidis, R. M. Stevenson, A. I. Tartakovskii, M. S. Skolnick, D. M. Whittaker, and J. S. Roberts. Parametric oscillation in a vertical microcavity: A polariton condensate or micro-optical parametric oscillation. *Physical Review B - Condensed Matter and Materials Physics*, 62(24):R16247–R16250, dec 2000.
- [4] A. Baas, J. Ph Karr, M. Romanelli, A. Bramati, and E. Giacobino. Optical bistability in semiconductor microcavities in the nondegenerate parametric oscillation regime: Analogy with the optical parametric oscillator [13]. *Physical Review B - Condensed Matter and Materials Physics*, 70(16):1–4, oct 2004.
- [5] J. Kasprzak, M. Richard, S. Kundermann, A. Baas, P. Jeambrun, J. M. J. Keeling, F. M. Marchetti, M. H. Szymańska, R. André, J. L. Staehli, V. Savona, P. B. Littlewood, B. Deveaud, and Le Si Dang. BoseEinstein condensation of exciton polaritons. *Nature*, 443(7110):409–414, sep 2006.
- [6] R. Balili, V. Hartwell, D. Snoke, L. Pfeiffer, and K. West. Bose-Einstein condensation of microcavity polaritons in a trap. *Science*, 2007.
- [7] Alberto Amo, Jérôme Lefrère, Simon Pigeon, Claire Adrados, Cristiano Ciuti, Iacopo Carusotto, Romuald Houdré, Elisabeth Giacobino, and Alberto Bramati. Superfluidity of polaritons in semiconductor microcavities. *Nature Physics*, 2009.
- [8] Giovanni Lerario, Antonio Fieramosca, Fábio Barachati, Dario Ballarini, Konstantinos S. Daskalakis, Lorenzo Dominici, Milena De Giorgi, Stefan A. Maier, Giuseppe Gigli, Stéphane Kéna-Cohen, and Daniele Sanvitto. Room-temperature superfluidity in a polariton condensate. *Nature Physics*, 2017.
- [9] K. G. Lagoudakis, M. Wouters, M. Richard, A. Baas, I. Carusotto, R. André, Le Si Dang, and B. Deveaud-Plédran. Quantized vortices in an excitonpolariton condensate. *Nature Physics*, 4(9):706–710, sep 2008.
- [10] Daniele Sanvitto and Stéphane Kéna-Cohen. The road towards polaritonic devices, 2016.
- [11] D. Ballarini, M. De Giorgi, E. Cancellieri, R. Houdré, E. Giacobino, R. Cingolani, A. Bramati, G. Gigli, and D. Sanvitto. All-optical polariton transistor. *Nature Communications*, 4(1):1778, jun 2013.
- [12] Félix Marsault, Hai Son Nguyen, Dimitrii Tanese, Aristide Lemaître, Elisabeth Galopin, Isabelle Sagnes, Alberto Amo, and Jacqueline Bloch. Realization of an all optical exciton-polariton router. *Applied Physics Letters*, 107(20):201115, nov



2015.

- [13] J.C López Carreño, C. Sánchez Muñoz, D. Sanvitto, and F.P. del Valle, E. anf Laussy. Exciting Polaritons with Quantum Light. *Physical Review Letters*, 115(19):196402, nov 2015.
- [14] Á. Cuevas, J.C.L. Carreño, B. Silva, M. De Giorgi, D.G. Suárez-Forero, C.S. Muñoz, A. Fieramosca, F. Cardano, L. Marrucci, V. Tasco, G. Biasiol, E. Del Valle, L. Dominici, D. Ballarini, G. Gigli, P. Mataloni, F.P. Laussy, F. Sciarrino, and D. Sanvitto. First observation of the quantized exciton-polariton field and effect of interactions on a single polariton. *Science Advances*, 4(4), 2018.
- [15] D. G. Suárez-Forero, V. Ardizzzone, S. F. Covre da Silva, M. Reindl, A. Fieramosca, L. Polimeno, M. de Giorgi, L. Dominici, L. N. Pfeiffer, G. Gigli, D. Ballarini, F. Laussy, A. Rastelli, and D. Sanvitto. Imaging the hydrodynamics of a single polariton. aug 2019.
- [16] A. Imamoglu, R. J. Ram, S. Pau, and Y. Yamamoto. Nonequilibrium condensates and lasers without inversion: Exciton-polariton lasers. *Physical Review A - Atomic, Molecular, and Optical Physics*, 1996.
- [17] Daniele Bajoni, Pascale Senellart, Esther Wertz, Isabelle Sagnes, Audrey Miard, Aristide Lemaître, and Jacqueline Bloch. Polariton laser using single micropillar GaAs-GaAlAs semiconductor cavities. *Physical Review Letters*, 2008.
- [18] Tsu-Chi Chang, Kuo-Bin Hong, Shuo-Yi Kuo, and Tien-Chang Lu. Demonstration of polarization control GaN-based micro-cavity lasers using a rigid high-contrast grating reflector. *Scientific Reports*, 9(1):13055, dec 2019.
- [19] S. Christopoulos, G. Baldassarri Höger Von Högersthal, A. J D Grundy, P. G. Lagoudakis, A. V. Kavokin, J. J. Baumberg, G. Christmann, R. Butté, E. Feltin, J. F. Carlin, and N. Grandjean. Room-temperature polariton lasing in semiconductor microcavities. *Physical Review Letters*, 2007.
- [20] Gabriel Christmann, Raphaël Butté, Eric Feltin, Jean-François Carlin, and Nicolas Grandjean. *Applied Physics Letters*, (5):051102, aug.
- [21] S. Kéna-Cohen and S. R. Forrest. Room-temperature polariton lasing in an organic single-crystal microcavity. *Nature Photonics*, 2010.
- [22] K. S. Daskalakis, S. A. Maier, R. Murray, and S. Kéna-Cohen. Nonlinear interactions in an organic polariton condensate. *Nature Materials*, 2014.
- [23] T. Guillet, M. Mexis, J. Levrat, G. Rossbach, C. Brimont, T. Bretagnon, B. Gil, R. Butté, N. Grandjean, L. Orosz, F. Réveret, J. Leymarie, J. Zúñiga Pérez, M. Leroux, F. Semond, and S. Bouchoule. Polariton lasing in a hybrid bulk ZnO microcavity. *Applied Physics Letters*, 2011.
- [24] Tien-Chang Lu, Ying-Yu Lai, Yu-Pin Lan, Si-Wei Huang, Jun-Rong Chen, Yung-Chi Wu, Wen-Feng Hsieh, and Hui Deng. Room temperature polariton lasing vs photon lasing in a ZnO-based hybrid microcavity. *Optics Express*, 20(5):5530, feb 2012.
- [25] Min Kyo Seo, Kwang Yong Jeong, Jin Kyu Yang, Yong Hee Lee, Hong Gyu Park, and Sung Bock Kim. Low threshold current single-cell hexapole mode photonic crystal laser. *Applied Physics Letters*, 2007.
- [26] Stefano Azzini, Dario Gerace, Matteo Galli, Isabelle Sagnes, Rémy Braive, Aristide Lemaître, Jacqueline Bloch, and D. Bajoni. Ultra-low threshold polariton lasing in photonic crystal cavities. *Applied Physics Letters*, 2011.
- [27] Masahiro Nomura, Naoto Kumagai, Satoshi Iwamoto, Yasutomo Ota, and Yasuhiko Arakawa. Photonic crystal nanocavity laser with single quantum dot gain. In *Optics InfoBase Conference Papers*, 2009.
- [28] Itamar Rosenberg, Yotam Mazuz-Harpaz, Ronen Rapaport, Kenneth West, and Loren Pfeiffer. Electrically controlled mutual interactions of flying waveguide dipolaritons. *Physical Review B*, 93(19):195151, may 2016.
- [29] P. M. Walker, L. Tinkler, M. Durska, D. M. Whittaker, I. J. Luxmoore, B. Royall, D. N. Krizhanovskii, M. S. Skolnick, I. Farrer, and D. A. Ritchie. Exciton polaritons in semiconductor waveguides. *Applied Physics Letters*, 102(1):012109, jan 2013.
- [30] Itamar Rosenberg, Dror Liran, Yotam Mazuz-Harpaz, Kenneth West, Loren Pfeiffer, and Ronen Rapaport. Strongly interacting dipolar-polaritons. *Science Advances*, 4(10):eaat8880, oct 2018.
- [31] Dror Liran, Itamar Rosenberg, Ken West, Loren Pfeiffer, and Ronen Rapaport. Fully Guided Electrically Controlled Exciton Polaritons. *ACS Photonics*, 5(11):4249–4252, November 2018.
- [32] Pavel Yu. Shapochkin, Maksim S. Lozhkin, Ivan A. Solov'ev, Olga A. Lozhkina, Yury P. Efimov, Sergey A. Eliseev, Vyacheslav A. Lovec'us, Gleb G. Kozlov, Anastasia A. Pervishko, Dmitry N. Krizhanovskii, Paul M. Walker, Ivan A. Shelykh, Maurice S. Skolnick, and Yury V. Kapitonov. Polarization-resolved strong light-matter coupling in planar GaAs/AlGaAs waveguides. *Optics Letters*, 43(18):4526, sep 2018.
- [33] M. W. Klein, T. Tritschler, M. Wegener, and S. Linden. Lineshape of harmonic generation by metallic nanoparticles and metallic photonic crystal slabs. *Physical Review B - Condensed Matter and Materials Physics*, 72(11), sep 2005.
- [34] Xinping Zhang, Shengfei Feng, Jian Zhang, Tianrui Zhai, Hongmei Liu, and Zhaoguang Pang. Sensors based on plasmonic-photonic coupling in metallic photonic crystals. *Sensors (Switzerland)*, 12(9):12082–12097, sep 2012.
- [35] Dominik A. Gollmer, Christopher Lorch, Frank Schreiber, Dieter P. Kern, and Monika Fleischer. Enhancing light absorption in organic semiconductor thin films by one-dimensional gold nanowire gratings. *Physical Review Materials*, 1(5), oct 2017.
- [36] P. S. Davids, B. A. Block, and K. C. Cadien. Surface plasmon polarization filtering in a single mode dielectric waveguide. *Optics Express*, 13(18):7063, sep 2005.
- [37] Harold Stoll and Amnon Yariv. Coupled-mode analysis of periodic dielectric waveguides. *Optics Communications*, 8(1):5–8, may 1973.
- [38] A. Yariv. Coupled-mode theory for guided-wave optics. *IEEE Journal of Quantum Electronics*, 9(9):919–933, sep 1973.
- [39] Amnon Yariv and Pochi Yeh. *Photonics: optical electronics in modern communications*. 2007.
- [40] B. R. Bennett, R. A. Soref, and J. A. Del Alamo. Carrier-induced change in refractive index of in p, gaas and ingaasp.

- IEEE Journal of Quantum Electronics, 26(1):113–122, Jan 1990.
- [41] Weng W. Chow and Dave Depatie. Carrier-induced refractive-index change in quantum-well lasers. Optics Letters, 13(4):303, apr 1988.
  - [42] S. Murata, A. Tomita, and A. Suzuki. Influence of free carrier plasma effect on carrier-induced refractive index change for quantum-well lasers. IEEE Photonics Technology Letters, 5(1):16–19, jan 1993.
  - [43] Orazio Svelto. Principles of lasers. Springer, Boston, MA, fifth edition, 2010.
  - [44] O. Jamadi, F. Reveret, P. Disseix, F. Medard, J. Leymarie, A. Moreau, D. Solnyshkov, C. Deparis, M. Leroux, E. Cambril, S. Bouchoule, J. Zúñiga Pérez, and G. Malpuech. Edge-emitting polariton laser and amplifier based on a ZnO waveguide. Light: Science and Applications, 2018.
  - [45] Hye Young Kim, Kangho Lee, Jae Woo Lee, Sangwook Kim, Gyu Tae Kim, and Georg S. Duesberg. Electrical properties of high density arrays of silicon nanowire field effect transistors. Journal of Applied Physics, 114(14):144503, oct 2013.
  - [46] Zhe Xiao, Tsung-Yang Liow, Jing Zhang, Ping Shum, and Feng Luan. Bandwidth analysis of waveguide grating coupler. Optics Express, 21(5):5688, mar 2013.
  - [47] S. M. Rytov. Electromagnetic properties of a finely stratified medium. Soviet Physics JETP, 1956.
  - [48] Ralf Bräuer and Olof Bryngdahl. Design of antireflection gratings with approximate and rigorous methods. Applied Optics, 33(34):7875, dec 1994.
  - [49] Lucio Claudio Andreani. Exciton-polaritons in superlattices. Physics Letters A, 192(1):99–109, aug 1994.
  - [50] Marco Liscidini, Dario Gerace, Daniele Sanvitto, and Daniele Bajoni. Guided Bloch surface wave polaritons. Applied Physics Letters, 98(12), mar 2011.

## Supporting Information

### EXPERIMENTAL SETUP

For all the optical characterization the sample is kept at cryogenic temperature of 4 K. All the PL measurements are realized in a confocal configuration, using a 100 fs pulsed laser with a repetition rate of 80 MHz, tuned at 1.59 eV ( $\approx 780$  nm) to excite the sample out of resonance. The detection system allows to reconstruct either real or Fourier spaces in a Charge Coupled Device (CCD) coupled to a monochromator 70 cm long with a diffractive grating with either 600 or 1800 lines per mm. This configuration gives spatial, angular and spectral resolution. An image of the real space is reconstructed before the CCD in order to apply a spatial filter by using a slit, enabling the selection of one or both gratings (as depicted in Figs. S6 and S7). A complete scheme of the experimental setup is displayed in Fig. S1. The residual laser signal is suppressed with a long-pass spectral filter at 1.55 eV ( $\approx 800$  nm). The time resolved images are performed in the same configuration, but directing the signal into a streak camera after passing the monochromator. The temporal reconstruction of the far field resolved in energy is made by moving vertically the focusing lens with a motorized station before it reaches the streak camera.

The energy dispersion is measured by imaging the Fourier plane of the objective lens that collects the light from the sample, as it is usually done when measuring polariton emission. The calibration of the emission wavevector in the propagation direction  $z$  depends on the magnification of such plane in the CCD camera and the objective lens working distance. This setup allows to individuate the angle ( $\theta$ ) at which the light is emitted from the grating, which is related to the wavevector by  $k_z = 2\pi \sin(\theta)/\lambda_o$ , where  $\lambda_o$  is the vacuum wavelength. Since the light is being extracted from the waveguide by the grating, exploiting the diffraction effect that couples the guided modes to radiative modes, the total wavevector of the confined mode associated to the detected light is given by [46]:  $\beta = k_z + 2\pi/\Lambda$  Where  $\Lambda$  is the grating periodicity.

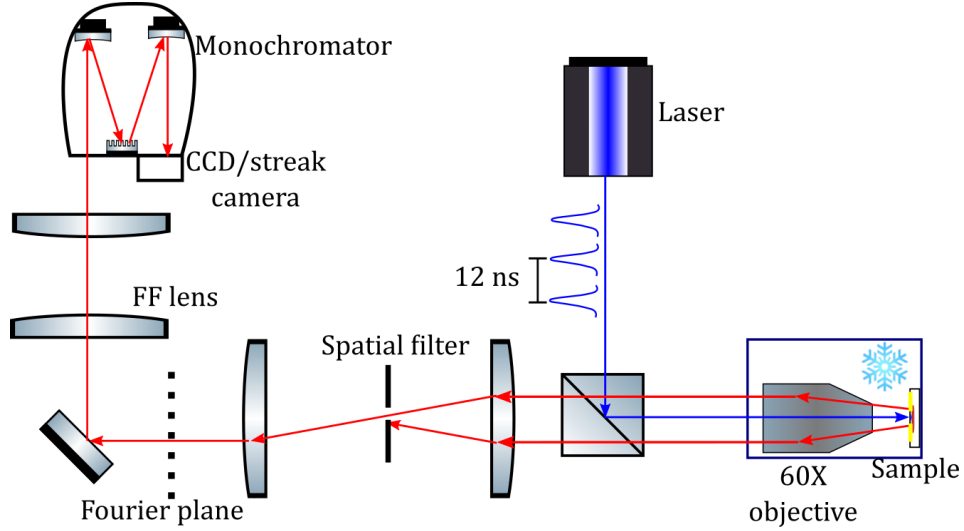


FIG. S1. Schematic representation of the experimental setup. The real space image of the sample emission is reconstructed at a given longitudinal position in order to apply a spatial filter, upon using a regulable micrometric slit. Afterwards the image of the real (Fourier) space is reconstructed on the camera by removing (inserting) the Far Field lens (FF lens).

### CALCULATION OF WAVEGUIDE MODES PROFILE AND GRATING COUPLED MODE ANALYSIS

To perform theoretical calculations on the perturbation induced by the grating on a guided mode, we use a semi-analytical model illustrated in Ref. [39]. It allows to find expressions for the electric and magnetic field distribution for an asymmetric waveguide composed by three homogeneous media. The periodic nature of our structure (12 pairs of QW+barrier) is taken into account by means of an effective index ( $n_{WG}^{eff}$ ) that weights the contribution of the two

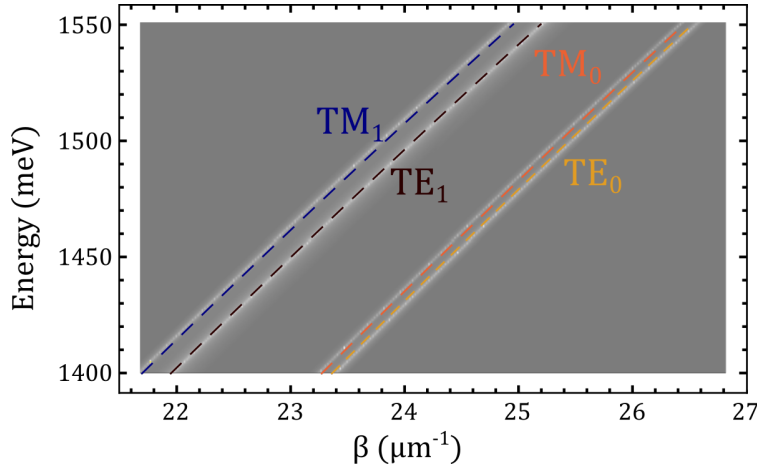


FIG. S2. Energy dispersions of the four guided modes supported by the structure, calculated using two different theoretical approaches: the background image (with the modes represented as white lines) corresponds to the dispersion calculated using the transfer matrix method, considering the internal structure of the waveguide, i.e., the 12 pairs of 20 nm layers of  $\text{Al}_{0.4}\text{Ga}_{0.6}\text{As}$  and GaAs. The dashed lines are calculated with the semi-analytical method illustrated in this section, assuming a mean effective index for the entire waveguide thickness. The good agreement between both calculations, validates the approximation of effective refractive index in the theoretical formalism used along the work.

constituent materials:  $\text{Al}_{0.4}\text{Ga}_{0.6}\text{As}$  ( $n = 3.30$ ) and GaAs ( $n = 3.54$ ). This approximation is justified by the fact that the layers are 20 nm thick, a size more than one order of magnitude below the wavelength of the photonic mode inside the structure ( $\lambda \sim 240 \text{ nm}$ ). The system is then operating in the “long wavelength” regime, in which the wave does not resolve in the structure [47, 48]. As a further validation of this approach, we compared the energy dispersion of the photonic modes by using a transfer matrix formalism that takes into account the periodicity of the waveguide. The results, presented in Fig. S2 confirm the pertinence of the formalism we use. They show a very good agreement between the two methods. However, the expressions obtained in the analytic formalism have the advantage to permit an accurate description of the interaction of the guided modes with the grating, hence, this is the formalism employed along the work.

In our calculations we use the expressions corresponding to an asymmetric waveguide of refractive index  $n_2 > n_3 > n_1$  defined in the spatial range  $-t < x < 0$ , with modes propagating in the  $z$  direction and infinitely extending along  $y$ . For this system the refractive indices correspond to:  $n_1 = n_{\text{ITO}}$ ,  $n_2 = n_{\text{WG}}^{\text{eff}}$  and  $n_3 = n_{\text{Al}_{0.8}\text{Ga}_{0.2}\text{As}}$ . The magnetic field ( $\mathcal{H}$ ) spatial profile of the  $\text{TM}_0$  mode can be written as:

$$\mathcal{H}_y(x) = \begin{cases} -C \frac{n_1^2 h}{n_2^2 q} \exp(-qx) & 0 \leq x \\ C \left( \frac{n_1^2 h}{n_2^2 q} \cos(hx) + \sin(hx) \right) & -t \leq x \leq 0 \\ C \left( \frac{n_1^2 h}{n_2^2 q} \cos(ht) + \sin(ht) \right) \exp(p(x+t)) & x \leq -t \end{cases} \quad (\text{S1})$$

Where the constants  $q$ ,  $p$  and  $h$  are chosen in order to satisfy the boundary conditions of the magnetic and electric fields and the wave equation for the electric field. The constant  $C$ , instead, determines the field’s intensity. The exciton resonance in the quantum well is taken into account by using a model of Lorentz oscillator [49, 50], in which the permittivity of the system in strong coupling is given by:

$$\epsilon(\omega) = \epsilon_\infty \left[ 1 + \frac{\omega_{LT}}{\omega_{ex} - \omega - i\gamma} \right] \quad (\text{S2})$$

Where  $\epsilon_\infty$  is the background dielectric constant,  $\omega_{ex}$  is the resonant energy,  $\gamma$  is the damping rate, and  $\omega_{LT}$  is the longitudinal/transverse splitting.

The insertion of a grating of refractive index  $n_g$ , height  $h$ , pitch factor  $\Lambda$  and filling factor  $a$  on top of the slab waveguide, can be treated as a perturbation of the polarization vector that couples a propagating mode with a counter-propagating one, by using the coupled-mode theory [38, 39]. In our case, the perturbation is a periodic binary

modulation of the refractive index, so it can be expanded in the Fourier basis as:

$$\Delta n^2(x, z) = \Delta n^2(x) \sum_{l=-\infty}^{\infty} a_l \exp(i2\pi lz/\Lambda) \quad (\text{S3})$$

$$\Delta n^2(x) = \begin{cases} (n_g^2 - n_1^2) & 0 \leq x \leq h \\ 0 & \text{elsewhere} \end{cases} \quad a_l = \begin{cases} \frac{1}{\pi l} \sin(\pi l a) & l \neq 0 \end{cases} \quad (\text{S4})$$

If a Fourier component  $a_q$  of the grating's spatial function is comparable with a guided mode's wavevector, i. e., if  $\beta_s \approx l\pi/\Lambda$ , the grating will couple the propagating mode with a counter-propagating one with opposite wavevector, following the behavior given by the equations system:

$$\frac{dA_s^-}{dz} = i\frac{\omega\mu}{4} a_q A_s^+ e^{i2(\pi q/\Lambda - \beta_s)z} \left( \frac{\epsilon_{Au}}{\epsilon_1} - 1 \right) \int_0^h [\mathcal{H}_y^s(x)]^2 dx \quad (\text{S5})$$

$$\frac{dA_s^+}{dz} = -i\frac{\omega\mu}{4} a_q A_s^- e^{-i2(\pi q/\Lambda - \beta_s)z} \left( \frac{\epsilon_{Au}}{\epsilon_1} - 1 \right) \int_0^h [\mathcal{H}_y^s(x)]^2 dx \quad (\text{S6})$$

Which can be written in a synthetic way as:

$$\frac{dA_s^-}{dz} = \kappa A_s^+ e^{-2\Delta\beta z} \quad (\text{S7})$$

$$\frac{dA_s^+}{dz} = -\kappa A_s^- e^{2\Delta\beta z} \quad (\text{S8})$$

Where  $|A^+(z)|^2$  and  $|A^-(z)|^2$  are the transverse field's intensity of the propagating and counter-propagating modes, respectively, at the position  $z$ . and the constants  $\Delta\beta$ , and  $\kappa$  are given by:

$$\Delta\beta = \beta_s - \pi q/\Lambda \quad \kappa = i\frac{\omega\mu}{4} a_q \left( \frac{\epsilon_{Au}}{\epsilon_1} - 1 \right) \int_0^h [\mathcal{H}_y^s(x)]^2 dx \quad (\text{S9})$$

## EFFECT OF THE GOLD GRATING ON THE TM POLARITONIC MODE

As a consequence of the periodic modulation of the refractive index, an energy gap centered at  $\omega(\beta_s = \pi q/\Lambda)$  is generated. As illustrated in the main text, we use gold gratings 30 nm high with a filling factor comprised between 0.72 and 0.85 and a pitch of 243 nm. Figures S3a-c show SEM images of a representative grating, taken at three different magnifications. In panels a and b it is possible to appreciate the irregular wire widths of the first few lines of the grating. This is a consequence of the higher dose at which the more dense features are exposed, a well known particularity of the nano-lithography technique used to fabricate the gratings (electron beam lithography), known as “proximity effect” [45]. The region affected comprises less than 1  $\mu m$ , though; a negligible portion compared to the full grating length (100  $\mu m$ ). An image taken with greater magnification in the central region of the grating is displayed in Fig. S3c, where the regular pitch can be appreciated. The small imperfections in the edges of each wire are in the order of units of nanometers, a scale well below the effective wavelength of the polaritonic mode ( $\sim 240$  nm) by around two orders of magnitude, making the irregularities negligible for the mode analysis. Panel d of the same figure displays the dispersion relation calculated according to the method illustrated above. The existence of the energy gap implies that the grating acts as a semi-reflective mirror in that spectral range.

Figure 1 of the main text and Fig. S4a show that the TM mode is broader than the TE mode, i.e., it is extracted with a lower angular resolution. To verify that this spread is not an intrinsic property of the waveguide, but rather a consequence of the interaction of the TM mode with the gold grating, the PL experiment is replicated, but this time, extracting the signal from a grating on top of the ITO, i.e., a less perturbative grating. As evidenced in Fig. S4 b, in this case both modes have comparable linewidths. This indicates that the broadening of the TM mode is a consequence of its interaction with the grating fabricated on top of the slab. It also indicates that the grating is much more perturbative for the TM mode than for the TE, in spite of the fact that the interaction is exclusively through the vanishing tail. As discussed in the main text, the stronger effect on the TM mode with respect to the TE, can be due to several effects such as a plasmonic resonance of the nanowires composing the grating or the proximity of the band gap to the excitonic resonance, the TM gap being closer to the energy range where the PL is more intense.

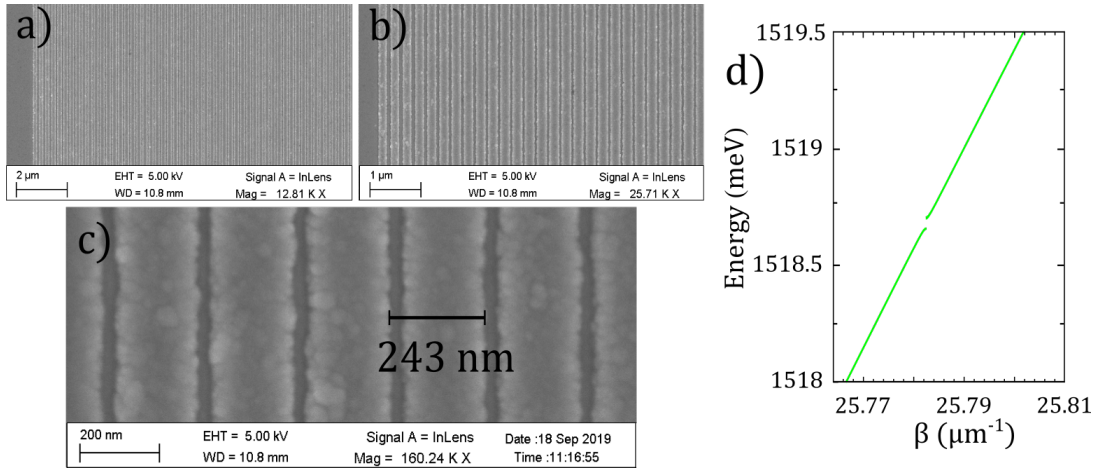


FIG. S3. **a-c** SEM images of a representative gold grating in the structure at three different magnifications: 13k (a), 26k (b) and 160k (c). Panels a and b show a proximity effect in the external part of the grating, due to the dense patterning of the structure. However, as observed in the same panels, after a few periods, the wire width regularizes. The more magnified image (panel c) give details on the structure parameters. It is characterized by a pitch of 243 nm and a filling factor comprised between 0.72 and 0.85. **d** A theoretical analysis indicates that the dispersion under the grating region is perturbed, and, as a consequence, an energy gap appears in the guided mode, which implies that the grating can act as a semi-reflective mirror for incoming WG modes with those energies.

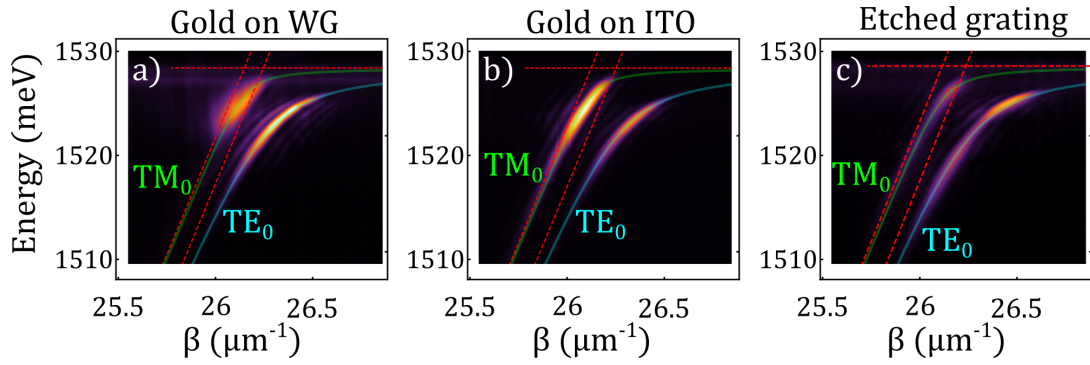


FIG. S4. Comparison of the PL spectrum of the guided modes extracted through three different gratings: **a** A metallic grating on top of the WG slab. Possible plasmonic effects manifest in the TM dispersion as a larger linewidth on the measured PL extracted from this grating. **b** A less perturbative grating on top of the ITO layer. The effect of the spread in  $\beta$  is suppressed. **c** To verify that no plasmonic effect is altering the detected WG dispersion, we perform the extraction from a dielectric grating etched on top of the slab surface.

The PL spectra extracted from gold gratings in contact with the slab and on the ITO capping layer are compared with a third PL measurement taken from a fully semiconductor grating. The results displayed in Fig. S4c confirm that the system is working in the strong coupling regime with the excitons of the QWs inside the WG, and discard the possibility of an apparent strong coupling induced by a coupling of the guided modes with a plasmonic resonance of the metallic grating.

A direct measurement of the energy gap introduced by the gratings is done by extracting the PL through a grating 400  $\mu\text{m}$  long, covering its first 100  $\mu\text{m}$  with a mask in the near-field as it is described in the main text.

## PROPERTIES OF THE LASER EMISSION

Figure S5 shows the main properties of the polariton laser demonstrated in this work. The panel S5a shows the total emitted intensity (black solid line) and full width at half maximum (FWHM, blue dashed line) of the lasing mode as a function of the pump power (see also Figures 3 and 4 of the main text). The FWHM is reduced when the pump power is increased and it reaches a minimum just above the lasing threshold. This behaviour is well known in

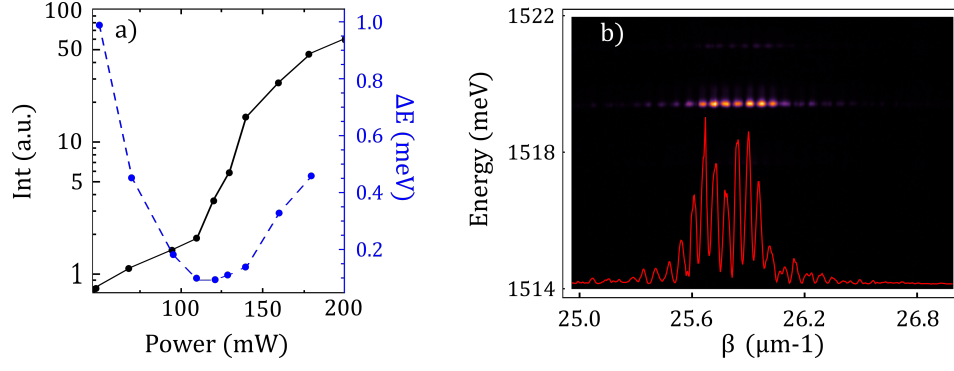


FIG. S5. **a** Emitted intensity (black solid line) and FWHM (blue dashed line) of the lasing mode upon increasing the pump power. A reduction in the linewidth at the lasing threshold is clearly visible. **b** Overlap in  $k$  space of the laser emission coming from the two gratings. The interference pattern results from the overlap of two coherent beams emitted by the two gratings.

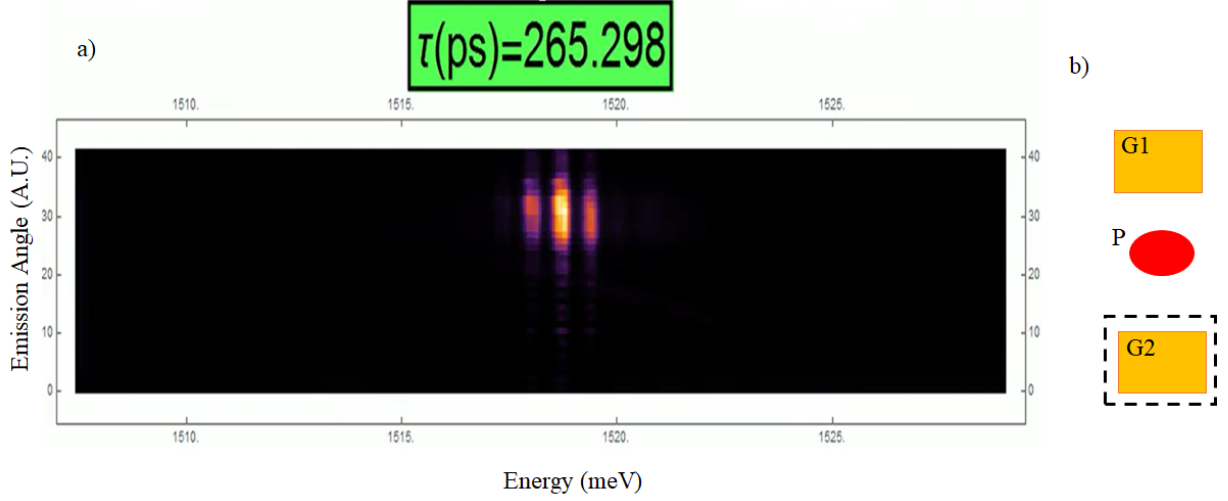


FIG. S6. **a** Screenshot from Video 1. A series of FP modes is visible in TM polarization, i.e., the polarization for which the two gratings act as mirrors. The excitation power is here close to the lasing threshold. **b** Scheme of the configuration used to obtain the data in **a**. The pump spot (P) is placed between the two gold gratings defining the FP cavity (G1 and G2). The light is collected only from one grating (indicated by the black dashed rectangle).

systems showing polariton lasing and it is explained as an increase of the coherence time above the lifetime of the polariton mode. At higher powers, a small increase of the FWHM is observed, which can be due to polariton-polariton and polariton-reservoir interactions. Figure S5b shows the overlap in the  $k$  space of the light emitted by the two gold gratings above the lasing threshold. The interference pattern is a hallmark of the first order coherence of the emitted laser light.

## TEMPORAL DYNAMICS

In this section we describe two screenshots from Supplementary Video 1 and Supplementary Video 2 and detail the way they are recorded. Each video is obtained from a  $k$ -space scan: for each  $k$  several hundreds of temporal series are acquired by using a streak camera. The set of data is then post-processed to obtain the temporal dynamics shown in the video. In other words, the data are grouped to obtain, from the intensity as a function of energy and time at a fixed  $k$ , the intensity as a function of energy and  $k$  at fixed time. The video is then obtained as a temporal series of such Intensity vs energy and  $k$  images.

Figure S6a shows a screenshot ( $\tau \approx 260$  ps) from Video 1. The data are acquired at an excitation power close to threshold and a series of lasing modes is still visible. The modes are in TM polarization, i.e., the polarization for



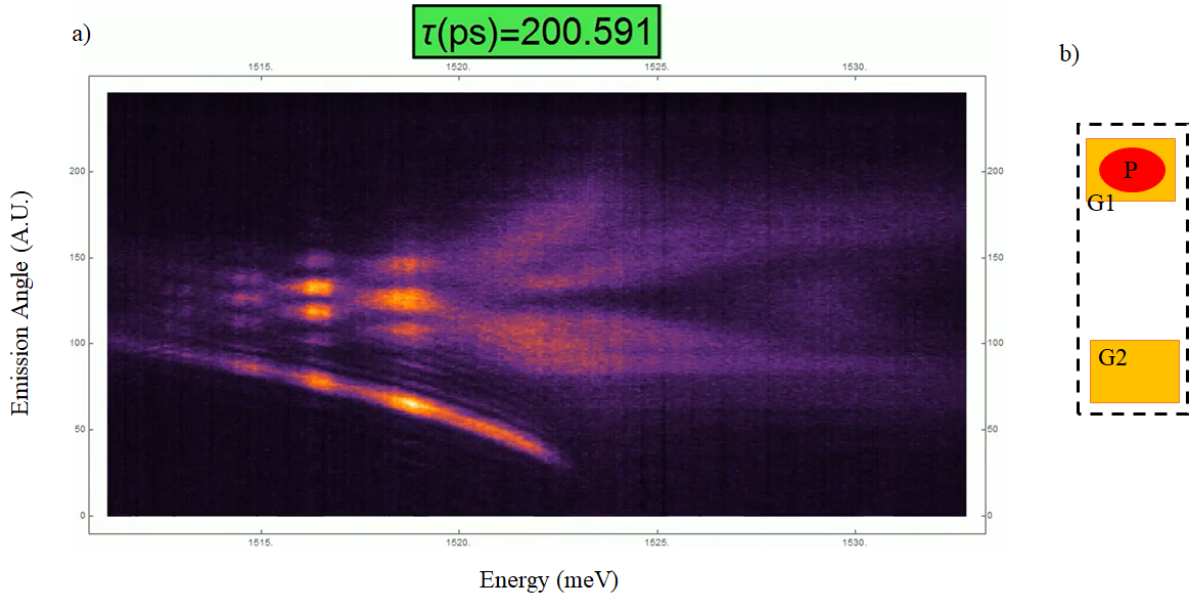


FIG. S7. **a** Screenshot from Video 2. This time the laser spot (P) is placed on one of the two gratings (G1) and the light is collected from both (black dashed line). The excitation power is here close to the lasing threshold and the overlap of light from the two gratings produce the interference pattern visible on the lasing modes. It is evident that the lasing starts to build-up when at least a spatial region of the sample (under the pumping spot) is in weak coupling. On the contrary, far apart from the pumping region the guided modes are strongly coupled with the exciton as it is shown by the TE dispersion coming from G2 (bottom of the screenshot); **b** Scheme of the configuration used to obtain the data in a. The pump spot (P) is placed on one (G1) of the two gold gratings defining the F.P. cavity (G1 and G2). The light is collected from both gratings (black dashed line).

which the two gold gratings act as mirrors in this configuration. Figure S6b shows the experimental configuration used to acquire the data of S6a. The pump spot (P) is placed between the two gold gratings G1 and G2 and the light is collected from the grating G2 only (black dashed line).

Figure S7a shows a screenshot ( $\tau \approx 200\text{ps}$ ) from Video 2. The data are acquired at an excitation power close to threshold and a series of lasing modes is still visible. In this case the light is collected from the whole cavity and the overlap in the  $k$  space produces an interference pattern. The discrete modes are in TM polarization, i.e. the polarization for which the two gold gratings act as mirrors in this configuration. Figure S7b shows the experimental configuration used to acquire the data of Fig. S7a and Video 2. The pump spot (P) is placed on grating G1 and the light is collected from the whole cavity (black dashed line). Interestingly, under the pumping spot the strong coupling is initially lost then slowly recovered. On the contrary, in the region of the sample corresponding to G2, i.e. far apart from the pump spot, the mode is always in strong coupling. See for instance the TE dispersion on the bottom, coming from G2. The data shown in S6 and S7 strongly suggest that the lasing effect we report here is triggered by a spatially localized population inversion (under the pump spot) coherently populating a manifold of polariton modes.

## APPLIANCE OF AN ELECTRIC FIELD

The effect of the electric field is the energy shift of the exciton peak by means of the Stark effect. As illustrated in Fig. 4a in the main text, the electric field shifts the excitonic resonance towards the modes of the Fabry-Perot resonator. As the exciton gets closer, the absorption, and hence, the quality factor of each mode is affected. At a voltage of 1.5 V the exciton peak is overlapped with the Fabry-Perot mode, increasing noticeably the absorption at this energy, and hence, reducing drastically the quality factor of the mode. Fig. S8 shows both effects. On the one hand, for applied voltages of 0.4 V and 0.9 V there is a shift of 0.02 meV and 0.12 meV, respectively. This demonstrates the possibility of a very fine tuning of the laser energy with the applied field. The spectrum corresponding to the highest applied field (1.5 V) shows how the change in the absorption peak affects the quality factor of the confined modes, inducing a spectral jump in the lasing energy, and hence, opening the possibility to use the applied electric field also as a switch to choose the desired lasing mode.

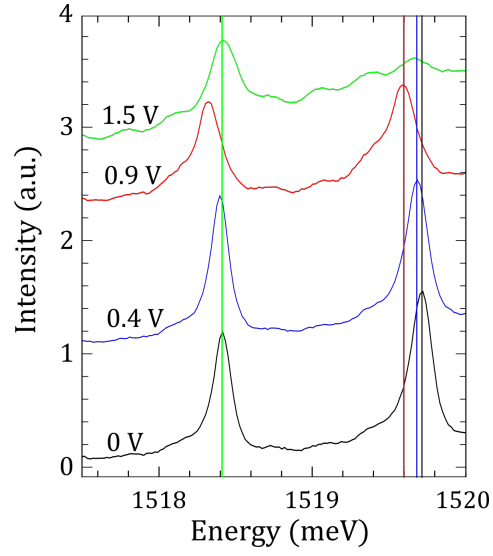


FIG. S8. By zooming the region of the cavity modes it is possible to identify the variations in the energy of the lasing mode (indicated by the vertical lines) for the different applied voltages. In the cases of 0.4 V and 0.9 V, the variation is small (0.02 meV and 0.12 meV, respectively), while in the case of 1.5 V there is an overlapping of the exciton with the bluest cavity mode; in this case the polariton lasing effect takes place in the consecutive one.